Journal of Water Process Engineering 72 (2025) 107647

Contents lists available at ScienceDirect

Journal of Water Process Engineering

journal homepage: www.elsevier.com/locate/jwpe

Study of photocatalytic and antimicrobial activities of TiO_2/ZnO/graphene oxide nanocomposites

Nidhi Verma [a,b], Tejpal Singh Chundawat [b,c], Harish Chandra [d], Monu Verma [e,f], Hyunook Kim [e], Dipti Vaya [g,*]

[a] Department of Sciences, HEC Group of Institutions, Haridwar, Uttrakhand, India
[b] Department of Applied Sciences, The NorthCap University, Gurugram, Haryana 122017, India
[c] Department of Chemistry, Guru Jambheshwar University of Science and Technology, Hisar, Haryana, India
[d] Department of Botany and Microbiology, Gurukul Kangri University, Haridwar, Uttrakhand, 249404, India
[e] Water-Energy Nexus Laboratory, Department of Environmental Engineering, University of Seoul, Seoul, 02504, Republic of Korea
[f] Department of Food Science and Technology, Graphic Era (Deemed to Be University), Dehradun, Uttarakhand 248002, India
[g] Department of Chemistry, Amity School of Applied Sciences, Amity University, Haryana 122413, India

ARTICLE INFO

Editor: Xiaying Xin

Keywords:
Photocatalytic activity
TiO_2-ZnO/ graphene oxide
Methyl Orange dye
Malachite green dye
Antibiotics

ABSTRACT

A simple and easy route was employed to synthesize TiO_2/ZnO (TZ) and TiO_2/ZnO/Graphene oxide (TZG) nanocomposites (NCs) followed by various characterizations using Powder X- Ray Diffraction (P-XRD), Field Emission Scanning Microscopy (FE-SEM), Energy dispersive X-Ray analysis (EDS), High-Resolution Transmission Electron Microscopy (HR-TEM), Raman and Ultraviolet-Visible Diffuse reflectance spectroscopy (UV–Vis-DRS) spectrophotometer. The P-XRD confirmed the formation of the anatase and zincite phases of TiO_2 and ZnO, respectively. The TZG NCs were evaluated for the removal of two antibiotics Amoxicillin (AMX) and Azithromycin (AZI) and two organic dyes Methyl Orange (MO) and Malachite Green (MG) *via* adsorption and photocatalytic degradation under solar-simulated light, achieving degradation efficiencies of 88 %, 50 %, 50.06 %, and 99.99 %, respectively. The degradation kinetics followed to the pseudo-second-order (PSO) kinetics model, with rate constant (k_2) 0.603×10^{-2},0.066×10^{-2} mol^{-1} L min^{-1} for AMX and AZI, respectively, while pseudo-first order (PFO) kinetics model with rate constant (k_1) 0.252×10^{-2} and 35.4×10^{-2} min^{-1} for MO and MG dyes, respectively. Antimicrobial activity tests of TZG NCs against bacteria Gram (+ve) *Staphylococcus aureus, Streptococcus sp.,* Gram (−ve) *Escherichia coli, Klebsiella pneumoniae, Pseudomonas aeruginosa and Salmonella typhi* showed good results for both Gram (+ve) and Gram (−ve) bacteria with Chloramphenicol antibiotic as a control drug. Among all tested bacteria, it showed a maximum inhibition zone for *P. aeruginosa* (23.0 ± 0.42 mm) among all tested microbial strains. These results indicated the remarkable advantages of TZG NCs for the degradation of antibiotics, dyes and antibacterial activity applications in wastewater treatment.

1. Introduction

Water contamination has emerged as a critical global challenge due to the combined effects of rapid population growth, urbanization, climate change, and inadequate water management [1]. This issue poses significant risks to both human health and ecological systems [2]. Among the key contributors of water pollution are, organic dyes [3], pesticides, herbicides, pharmaceuticals [4], and pathogenic bacteria [5]. Organic dyes are highly toxic due to their carcinogenic and non-biodegradable in nature and are widely used in textiles, paper, plastics industries, *etc.* [6]. Antibiotics are broad-spectrum active compounds [7], chemotherapeutic agents [8], and also developed antibiotic-resistant bacteria [9]. In past years, due to the endemic and different pandemic crises [10,11], the production of antibiotics and their utilization by humans and animals has increased exponentially [12].

Therefore, there is a need to develop an effective material and method that can remove pollutants and act as antimicrobial agents. For this purpose, heterogeneous catalysis *via* photocatalytic activity would be performed a significant role. In the photocatalytic process, semiconductors are used as a photocatalyst and oxidizing radicals such as hydroxyl and super oxides radicals are produced which efficiently oxidize pollutants as well as played an important role in disinfection of

* Corresponding author.
E-mail address: diptivaya08@gmail.com (D. Vaya).

https://doi.org/10.1016/j.jwpe.2025.107647
Received 14 September 2024; Received in revised form 29 March 2025; Accepted 2 April 2025
Available online 7 April 2025

Table 1
Comparison of different antibiotics removal with other sorbents.

Materials	Pollutants	Time	% degradation	References
Au/MIL101(Fe)/BiOBr	Norfloxacin	75 min	81. 8 %	[45]
MIL-101(Fe)/BiOBr	Enrofloxacin	45 min	84.4 %	[46]
$Ag/Ag_6Si_2O_7/Bi_{12}O_{17}Cl_2$	Tetracyclin	60 min	82.8 %	[47]
	Levofloxacin	100 min	85.1	
Bi_2WO_6/C_3N_4/carbon fiber cloth composite	Tetracyclin	90 min	84.4 %	[48]
	Oxyteracyclin	–	97.5 %	
	Norfloxacin	–	71.4 %	
	Ciprofloxacin	–	81.2 %	
$Mn_{0.5}Cd_{0.5}S$/BiOBr	Oxytetracyclin	75 min	92.4 %	[49]
$Cd_{0.5}Zn_{0.5}S$ nanoparticles/ Bi_2MoO_6 microspheres/carbon dots	Oxytetracyclin	40 min	92.4 %	[50]
$Ag/Ag_3PO_4/C_3N_5$	Levofloxacin	90 min	84.7 %	[51]
Scallop shell coated Fe_2O_3	Tetracyclin	–	–	[52]
Biochar of pine bar	Tetracyclin	15 min	89.5 %	[53]
$Mn_{0.5}Cd_{0.5}S/Bi_2MoO_6$	Tetracyclin	60 min	90.7 %	[54]
$BiOBr/N\text{-}C_3N_5$	Tetracyclin	90 min	81.7 %	[55]

microorganisms [13]. These are cost effective, environment friendly and easy to handle [14]. Previously, different metal, metal oxides and their nanocomposites such as TiO_2 [15], ZnO [16] TiO_2-GO [17] and TiO_2/ZnO/rGO [18] *etc.* are reported in the degradation and mineralization of several contaminants including dyes and antibiotics. Li et al. removed tetracycline (TC) antibiotics by GO/Titania composite to from aqueous solution [19]. Further, Tabrizian et al. removed TC *via* adsorption by preparing bimetallic nanocomposites (Fe/Cu-GO) [20]. Recently, Rajkumari *et. al* degraded the Rhodamine B and Amoxycillin by TiO_2/GO and ZnO/GO NCs and found that Amoxycillin more degraded by TiO_2/GO in comparison to ZnO/GO while both show similar efficiency for Rhodamine B [21]. Manda *et. al* efficiently degraded MB dye up to 98.5 % by ZnO/TiO_2/rGO NCs. They varied the concentration of rGO in (5, 10 and 20 %) to degrade the MB dye contaminants and found that 5 % rGO (ZnO/TiO_2/rGO NCs) was more efficient [22]. Recently, Rudd et al. synthesized Tantalum nitride (Ta_3N_3) as aphotoelectrode materials [23].

Both the metal oxides ZnO and TiO_2 have almost similar band gap (approximately 3.2 eV), similar photocatalytic mechanism, high active sites, size tuning, environment friendly, and low cost, which make them suitable candidates as a good photocatalyst [24]. These also have excellent oxidizing and reducing potential due to the photo-induced e^-/h^+ pair which are responsible for effective photocatalytic efficiency in the presence of light irradiation [25,26]. The combination of ZnO and TiO_2 decline the recombination of e^-/h^+ pair under UV light irradiation and therefore synergetic effect of both metal oxides are responsible for greater photocatalytic activity [27]. Due to all mentioned reasons ZnO/TiO_2 binary nanocomposites are being considered as an encouraging photocatalyst [28]. Both materials also exhibited good antimicrobial activity against both strain of Gram (+ve) and (−ve) bacteria. ZnO/TiO_2 nanocomposite has shown excellent antimicrobial activity against both type of strain of bacteria as compared to ZnO [29]. Although semiconductor materials are considered very good photocatalyst, but these also possess some drawbacks such as fast recombination of e^-/h^+ pair, large band gap and band gap energy not tuned with visible light range which leads to insufficient photocatalytic degradation of pollutants and limit its application as a catalyst in real wastewater on large scale [30].

To enhance the catalytic efficiency and to lessen the drawbacks in semiconductors, the carbon-based materials doping [31,32], hybrid materials [33], and hydrogenation [34] like modification are extensively used. Among all, graphene oxide (GO) has been widely applicable for suppression of recombination of e^-/h^+ pair due to having greater surface area, high conductivity, and movement of charge carriers [17,35,36]. It also increased the interaction between catalyst and pollutants [37], expanded spectrum of light absorption towards visible range [38], and showed antimicrobial activity by wrapping and act as cutter for bacterial cell [39].

Amoxicillin (AMX), is semisynthetic [40] and β-lactam antibiotic which is act as a barrier for bacterial cell wall formation [41]. Azithromycin (AZI) is toxic and macrolide semisynthetic antibiotic [9]. AMX and AZI are used on large scale as a medicine, and their elimination is very low due to slow metabolism [42]. On the other hand, MG dye is water soluble triphenyl methane cationic dye [43], while MO dye is water-soluble azo anionic dye [44]. The biological pathogens which are chosen such as *K. pneumonias, P. aeruginosa and S. typhii* are responsible for pneumonia, blood- infection, lungs (pneumonia) and typhoid fever respectively. On the basis of above reasons, all these were selected as model contaminants.

Comparative study of different materials catalytic activity is given in Table 1.

In present work, binary TiO_2/ZnO (TZ) and ternary TiO_2/ZnO/Graphene oxide (TZG-NCs) nanocomposite are prepared *via* simple and easy chemical approach, and studied first time for the photodegradation capability onto two antibiotics as AMX, AZI and two organic dyes as MO and MG. The antimicrobial activities were also investigated against both strain of bacteria. In last section, tentative dye degradation mechanism was also proposed.

2. Experimental

2.1. Materials

Details are given in supplementary file.

2.2. Graphene oxide (GO) preparation

Graphene oxide (GO) was synthesized from graphite powder using a modified Hummers method. Briefly, 2 g each of graphite powder and $NaNO_3$ and concentrated H_2SO_4 mixed properly. The reaction mixture was placed under ice bath. Then, 6 g of $KMnO_4$ was gradually added. Afterward, 20 mL of 30 wt% H_2O_2 solution was added and resulting product was separated and dried in an oven at 65 °C [56].

2.3. Synthesis of TiO_2/ZnO binary nanocomposites (TZ-NCs)

Binary TZ-NCs were synthesized using the sol-gel method. Initially, 2 g of zinc acetate dihydrate was dissolved in 20 mL of ethanol and stirred at room temperature for 4 h. Subsequently, 20 g of titanium isopropoxide (TTIP) was gradually added to the solution, with stirring continued until a gel formed. The gel-like material was then washed with deionized water and ethanol before being placed in an oven at 100 °C for 12 h. A white powder material was TZ NCs [57].

2.4. Synthesis of TiO_2/ZnO/GO ternary nanocomposites (TZG-NCs)

To prepare TZG-NCs, 1.0 g of binary TZ-NCs were dispersed in 10 mL ethanol followed by stirring and ultrasonication to form homogenous solution (solution I). On the other hand, 100 mg GO was dispersed also in 1 mL ethanol and followed by ultrasonication to homogenise (solution II). Solution II was added in solution I slowly by stirring and ultrasonication to form homogenous mixture. The grey coloured

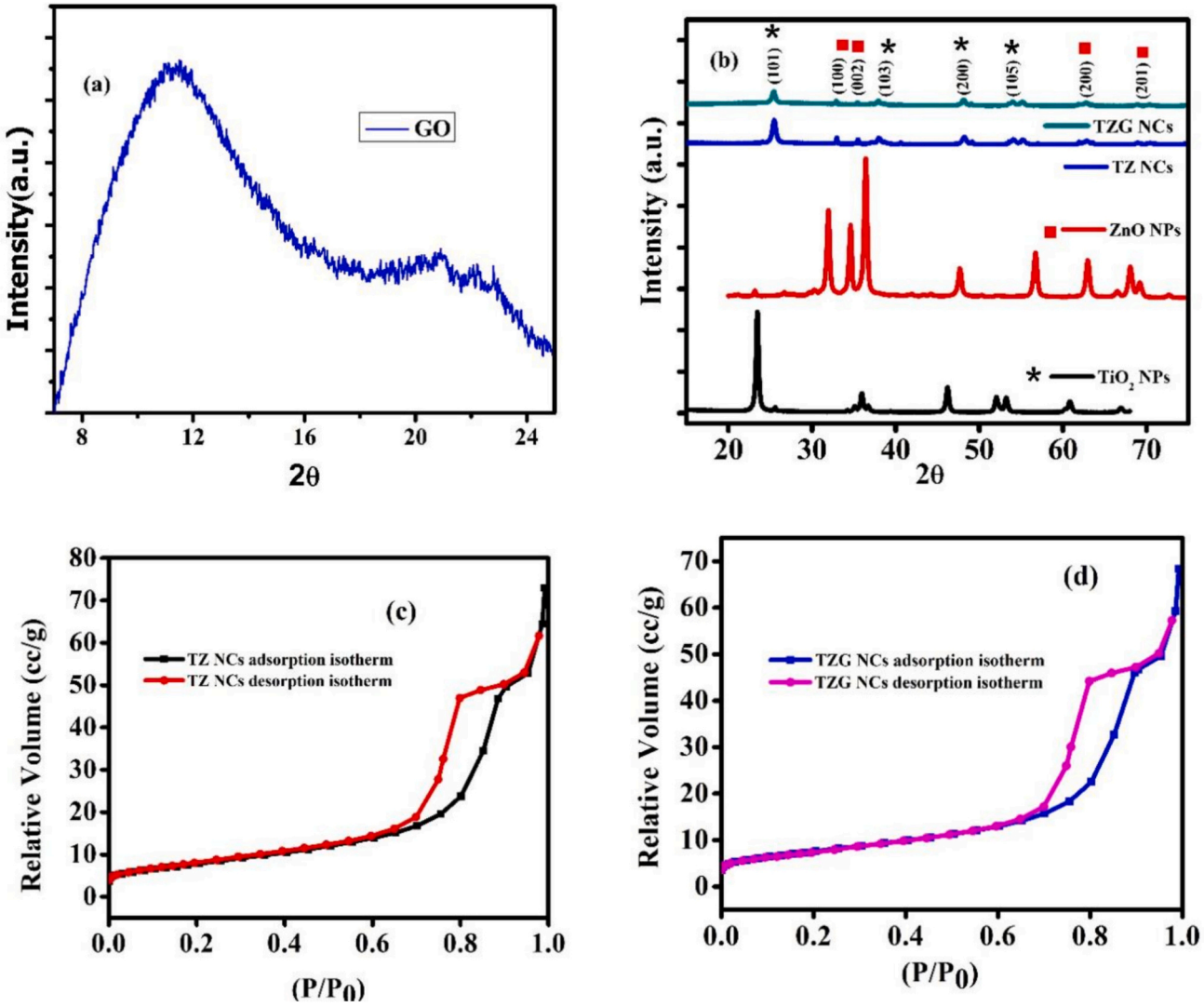

Fig. 1. P-XRD (a)-(b) Nitrogen adsorption-desorption isotherms(c)-(d).

homogenous solution was formed which is centrifuged by DI water and ethanol. Further it was dried up to 400 °C in furnace for 3 h to get TZG-NCs.

2.5–2.8 Procedure of Photocatalysis and antimicrobial activity and characterization given in supplementary file.

3. Results and discussion

3.1. P-XRD analysis

The P-XRD patterns of synthesized GO, TZ and TZG-NCs are given (Fig. 1 a and b). GO (Fig. 1 a) shows broad peak at (2θ) 10.3° confirming the formation of GO from graphite powder.

Bragg's formula Eq. (1) was used to calculate the inter-planar spacing, which was 0.789 nm, confirmed a random packing of graphene sheets in the GO.

$$N\lambda = 2d\sin\theta \quad (1)$$

Where, n is denoted as positive integer, λ is wavelength of incident wave, θ is glancing angle and d is inter-planar distance.

The P-XRD diffraction peaks of TZ-NCs displayed at 2θ with respective planes as resemble anatase phase of TiO_2 are 25.43^0 (101), 38.05^0 (103), 48.00^0 (200), 55.20^0 (105) (JCPDS no.: 21–1272), while 32.93^0 (100), 35.49^0 (002), 62.98^0 (200), and 68.01^0 (201) correlates with zincite phase of ZnO respectively (JCPDS no.: 36–1451), which confirms the high crystallinity. The displacement of peak anatase (101) is due to lattice contraction in TZ and TZG NCs. The average crystallite size calculated by Scherrer formula [58] of TZ-NCs was found approximate 21.18 nm. The P-XRD pattern of TZG-NCs revealed the diffraction peaks nearly same theta as TZ-NCs with low intensity, due to the inclusion of GO. The average crystallite size of TZG-NCs was found 16.60 nm which is lesser than TZ-NCs. This is probably due to TiO_2 and ZnO NPs interaction with GO matrix as previously reported [59]. The peak of GO is not exist in P-XRD of TZG-NCs, this might be due to good exfoliation of GO and lesser amount (10 % GO) used in the composite preparation [60,61].

The lattice parameters (a, c) along with unit cell volume (V), microstrain (ε), dislocation density and stacking fault of synthesized TZ and TZG NCs are calculated by (Eq. 1S–5S). All parameters are enlisted in (Table 2S and 3S).

3.2. BET surface area

The N_2 adsorption-desorption measurements were performed to determine the specific surface area, pore volume and pore size distribution of the prepared TZ and TZG NCs nanocomposites. Fig. 1c, d showing the N_2 adsorption-desorption isotherms for the prepared samples and textural data are given in Table 4S. Data showed type IV

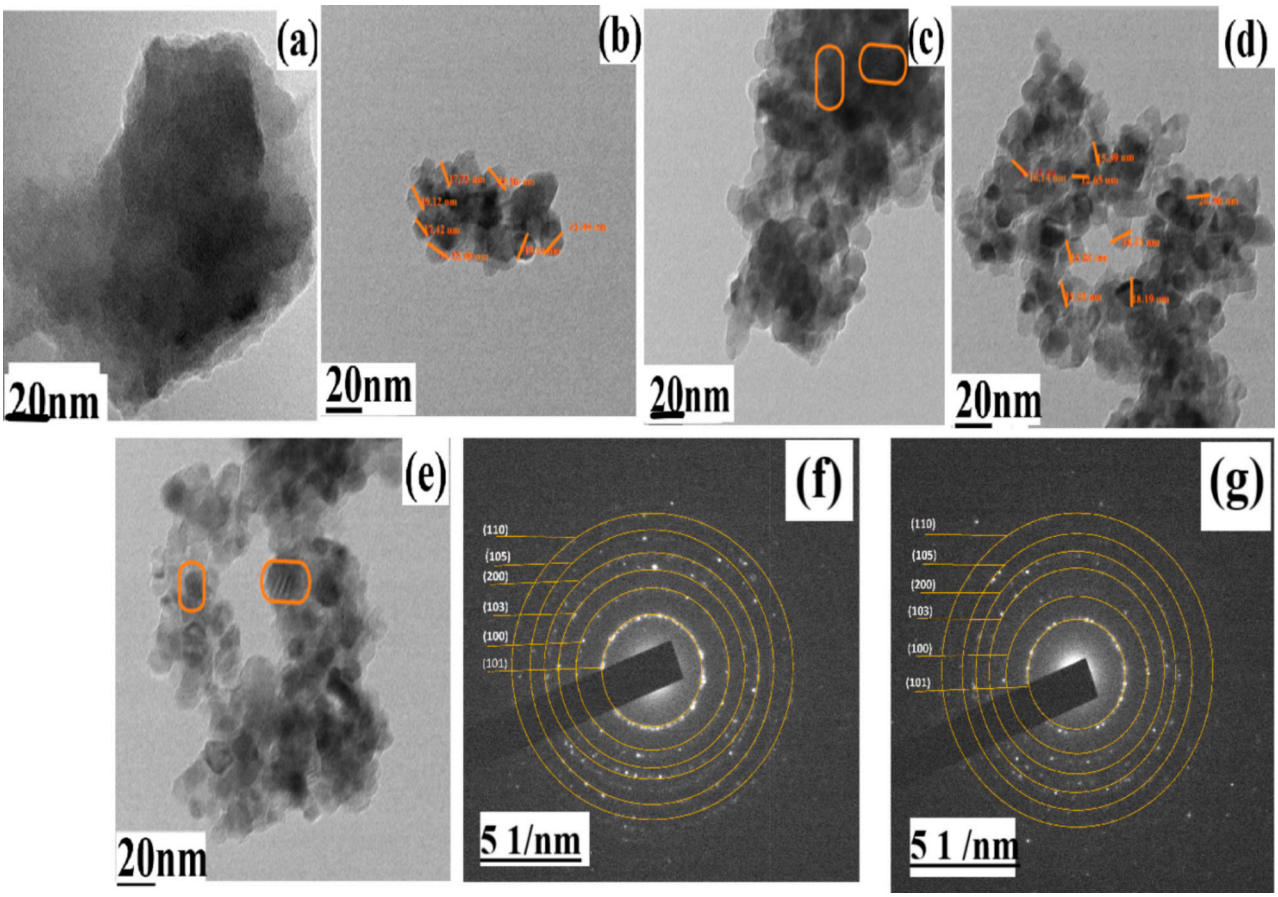

Fig. 2. HR-TEM Images: a) GO. b, c) TZ (20 nm). d, e) TZG-NCs (20 nm). SAED pattern: f) TZ. g) TZG-NCs.

isotherm with hysteresis loops type H3, indicating the mesoporous structure. The BET surface area, cumulative pore volume and average pore sizes were calculated and reported in Table 4S. This large surface area and porosity of composites favored the adsorption and photocatalytic activity application.

3.3. FE-SEM and SEM-EDX analysis

FE-SEM images of GO, TZ and TZG-NCs are displayed in (Fig. 1S a-e). GO showing a sheet type structure with overlapping to each other as shown in (Fig. 1S a). TZ-NCs showing both TiO_2 and ZnO NPs contain spherical shape (Fig. 1S b and c). In TZG NCs both TiO_2 and ZnO NPs are scattered over the GO layer to form a compact structure and morphology of TZ NCs is changed due to the insertion of GO (Fig. 1S d and e).

In EDS (Fig. 2S a and b) of TZ and TZG-NCs include Ti, O and Zn at specific position which confirms pure form of compounds. There was no other peak was observed, confirmed the high purity of the synthesized both NCs. In TZG-NCs, carbon peak (C) is also observed due to GO in TZG NCs (Fig. 2S b).

3.4. HR-TEM analysis

HR-TEM analysis was further investigated to know more deeply about the morphologies, average size and crystallographic structures of prepared GO, TZ-NCs and TZG-NCs as shown in (Fig. 2 a-g). The HR-TEM (Fig. 2 a) image of GO showing sheet like morphology overlapped to each other. The TEM images of TZ-NCs (Fig. 2 b and c) indicating the aggregation between TiO_2 and ZnO due to partial charges. The TEM images of TZG-NCs (Fig. 2 d and e) showing that TiO_2 and ZnO are speared over GO nanosheet in agglomerated form which makes a compact structure. As the activity of the photocatalytic materials is depend upon intrinsic band structures, specific surface area and particle size "Higher degree of crystallinity higher will be the photocatalytic activity" [62] and it is confirmed from the TEM images that there was good interaction among the TiO_2, ZnO and GO in the nanocomposites which is good for photocatalytic activity. The selected-area electron diffraction (SAED) patterns (Fig. 2 f and g) patterns of the TZ and TZG-NCs confirmed that both materials have good crystallinity and polycrystalline in nature because of multiple ring type structures and confirm the indexing with P-XRD. The lattice fringes in (Fig. 2 c and e) are not in same directions which confirms the polycrystalline nature of TZ as well as TZG-NCs respectively. The calculated average particle size of TZ-NCs was 138.57 nm (calculated by using image J software). On the inclusion of GO in TZG-NCs, the crystallinity reduced upto some extent while remained polycrystalline in nature (Fig. 2 f and g). Calculated average particle size of TZG-NCs was 104.71 nm.

3.5. Raman analysis

Raman spectra of samples GO, TZ and TZG NCs (10 wt% GO) were presented in (Fig. 3S a and b). The two prominent bands were exhibited at 1363 cm^{-1} (D band) and 1608 cm^{-1} (G band) which resembles GO. (Fig. 3S b). Bands matching to anatase phase of TiO_2 at around 144 ($Eg_{(1)}$), 393 (B_1g (1), 513 (A_1g), and 642 cm^{-1} E_g (3), in TZ as well as in the TZG NCs respectively. TiO_2-ZnO peak at 313 cm^{-1} appeared in TZG NCs [63] (Fig. 3S a). The relative intensity declines in the TZG NCs as compared to TZ NCs which is due to the insertion of GO. The clear peak of ZnO is not visible here. The Raman data have been taken of TZ NCs between 200 and 800 while TZG NCs upto 1800 cm^{-1}.

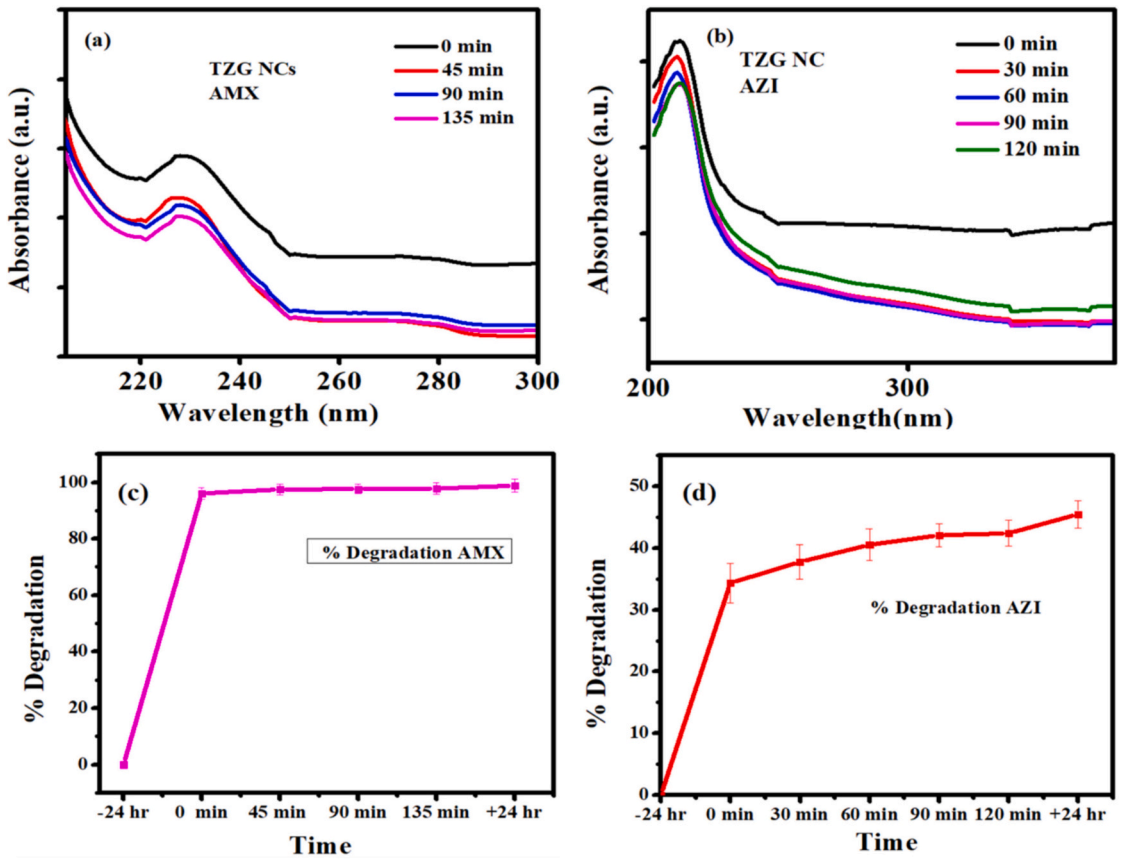

Fig. 3. Photocatalytic degradation: a and c) AMX by TZG-NCs. b and d) AZI by TZG-NCs.

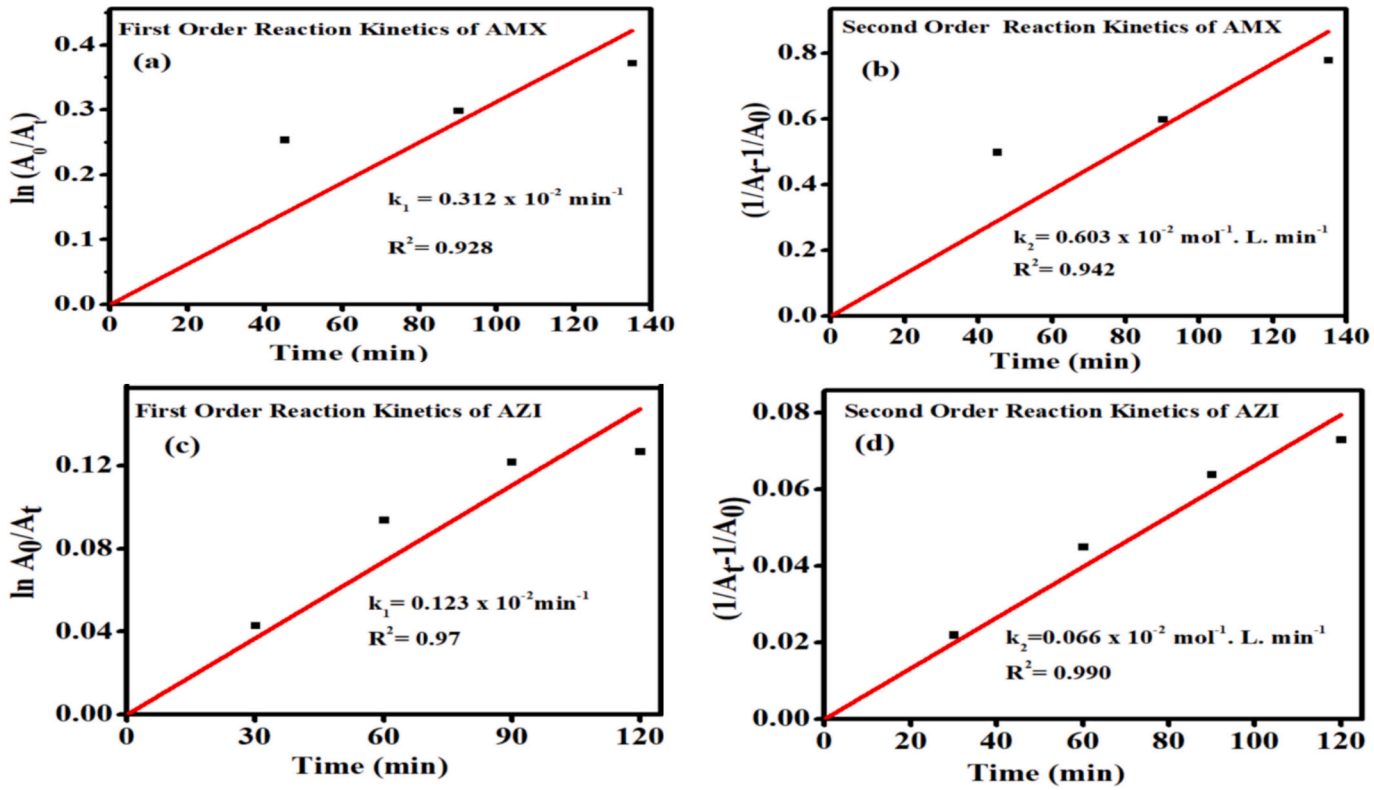

Fig. 4. a-d Kinetic data fitting for AMX and AZI antibiotics with TZG-NCs.

Table 2
PFO and PSO kinetics parameters of AMX, AZI, MO, and MG pollutants degradation in presence of TZG-NCs.

Pollutants	Time (min)	% Degradation	PFO		PSO	
			k_1 (min^{-1})	R^2	k_2 (mol^{-1}. L. min^{-1})	R^2
AMX	135	88	0.312×10^{-2}	0.928	0.603×10^{-2}	0.942
AZI	120	50	0.123×10^{-2}	0.970	0.066×10^{-2}	0.990
MO Dye	200	50.06	0.252×10^{-2}	0.939	0.434×10^{-2}	0.915
MG Dye	11	99.99	35.40×10^{-2}	0.954	496.7×10^{-2}	0.953

3.6. Zeta potential

The stability of photocatalysts were investigated by zeta potential. The value of zeta potential of GO, TZ and TZG NCs were − 40, −10.5 and − 12 mV respectively (Fig. 4S). All 3 prepared nanomaterials are having negative zeta values, which is favourable for the removal of cationic dyes such as MG.

3.7. UV- visible spectrum and Kubelka Munk function

The reflection spectra of TZ and TZG NCs were recorded UV–Vis DRS and data is presented in (Fig. 5S). The band gap data of the NCs were found by plotting the graph as shown in (Fig. 5S a- b), and calculated by Kubelka Munk function Eq. (2) as given below:

$$\frac{K}{S} = \frac{(1 - R_\infty)^2}{2R_\infty} \equiv F(R_\infty) \quad (2)$$

Where, R_∞ = diffuse reflectance, ($F(R_\infty)$ = Kubelka Munk function, h = Planck constant, ν = frequency, K = molar absorption coefficient, S = scattering factor.

The calculated band-gap energy was 3.5 eV and 3.4 eV for TZ and TZG-NCs respectively. Although, the difference between the band gap values for these both NCs are lesser but is lower for TZG-NCs. The presence of oxygen-containing functional groups and the electronic interaction between the nanoparticles and GO layers lead to an upward shift in the valence band edge. This shift enhances light absorption and reduces the band-gap energy of the nanocomposites. Uniform dispersion of TiO_2 and ZnO nanoparticles (NPs) on the surface of GO results in the formation of TZG NCs, which improves light absorption and boosts photocatalytic efficiency in degrading organic pollutants [64].

3.8. Photocatalytic degradation of AMX and AZI by TZG-NCs

The photocatalytic degradation was carried out under solar-simulated light illumination and the activity was measured by UV–Vis spectrometer. Absorbance values were declined with reaction time due to photocatalytic degradation as indicated in (Fig. 3 a-b), and their respective degradation efficiencies are shown in (Fig. 3 c-d) according to the following Eq. (3):

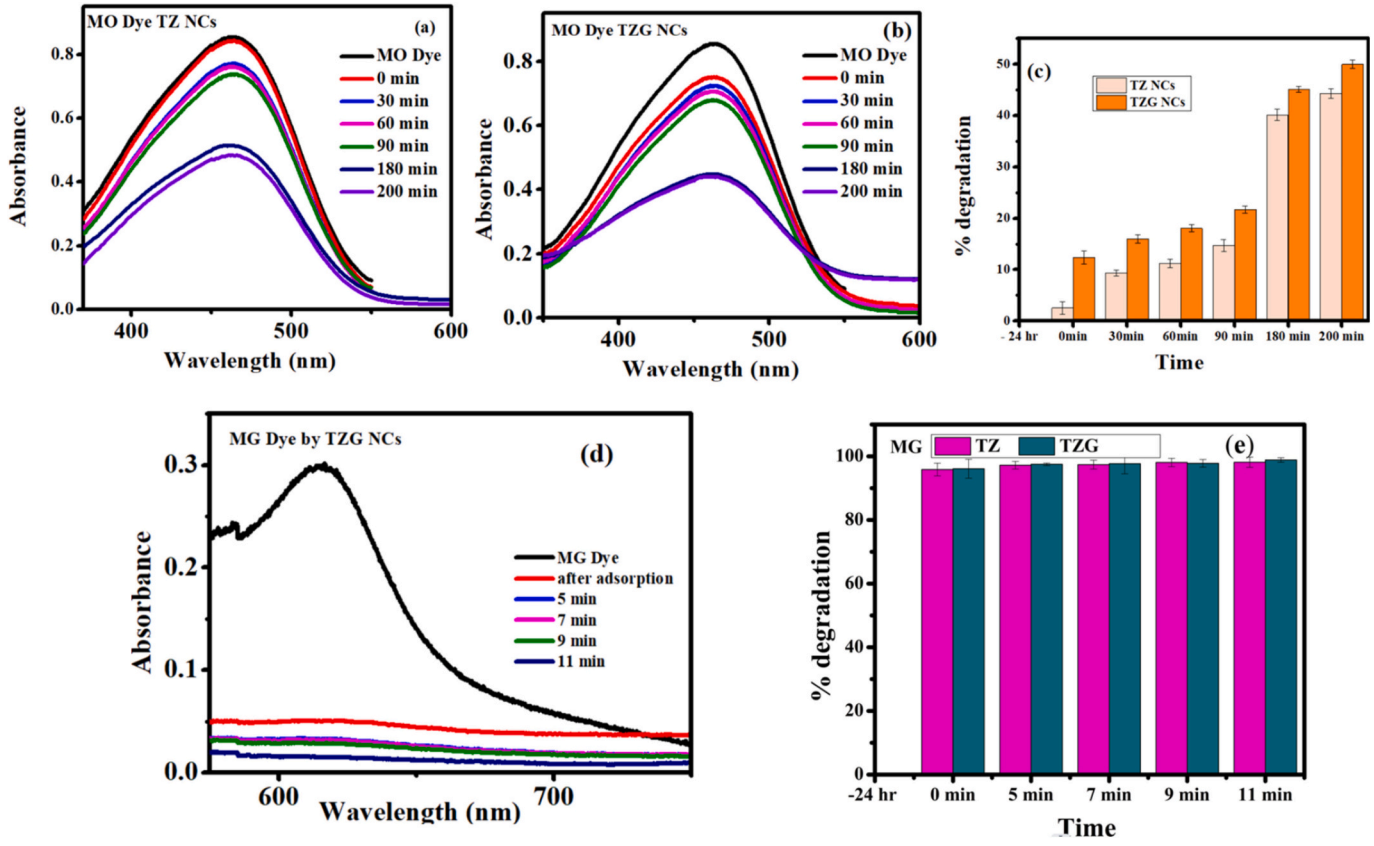

Fig. 5. Photocatalytic activity: a-c) MO dye; d- e) MG dye.

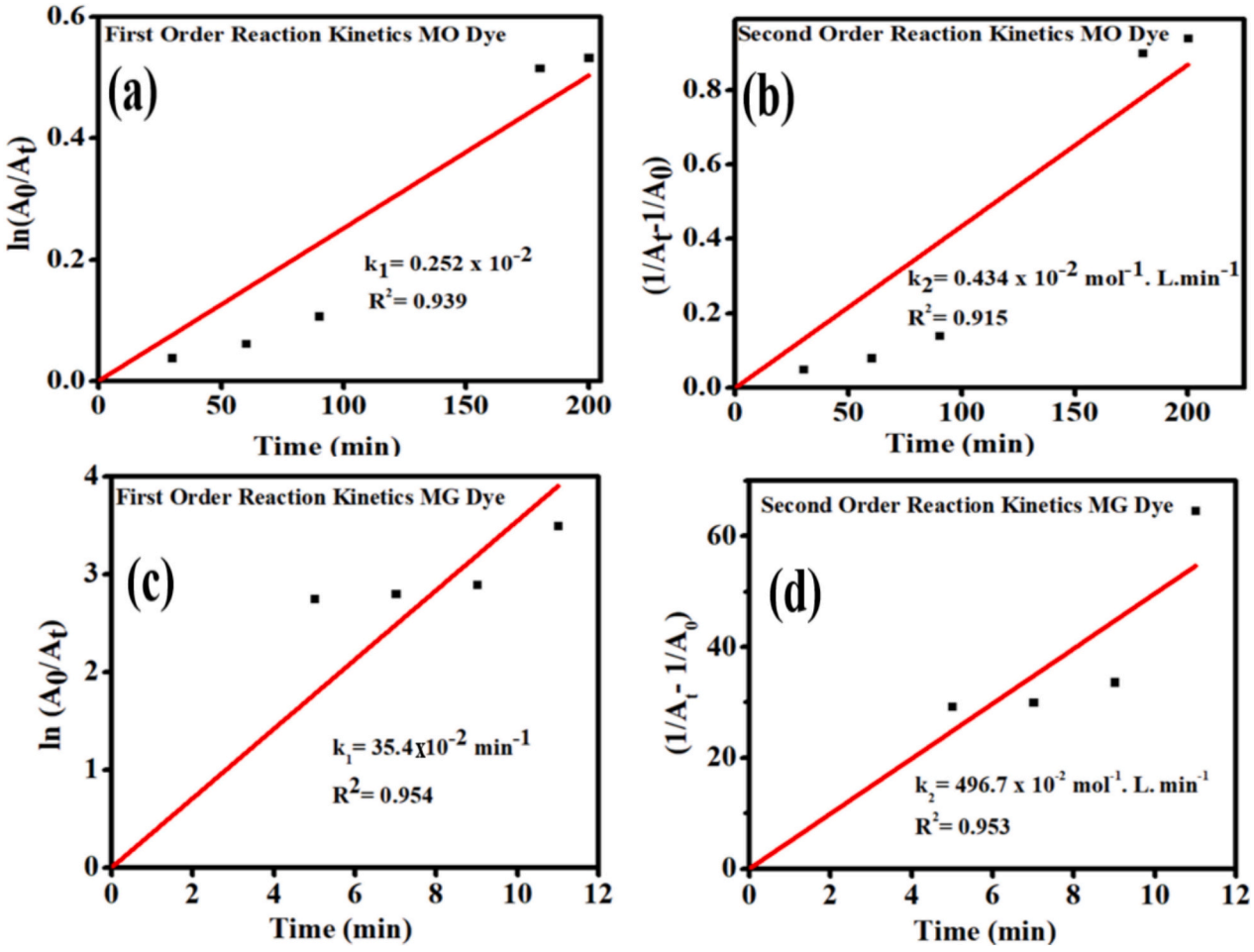

Fig. 6. a-d Kinetic data fitting TZG-NCs.

$$\%\text{Degradation} = \frac{A_o - A_t}{A_o} \times 100 \quad (3)$$

Where, A_0 = initial absorbance and A_t = absorbance after photocatalytic degradation respectively.

It has been observed that the adsorption and degradation of AMX was completed upto 88 % within 135 min while in case of AZI, it was upto 50 % were observed in 120 min by TZG-NCs. The kinetic data were analyzed using two models: the pseudo-first-order (PFO) and pseudo-second-order (PSO), represented by eqs. (4) and (5), respectively.

$$k_1 t = ln\left(\frac{A_o}{A}\right) \quad (4)$$

$$k_2 t = \left(\frac{1}{A} - \frac{1}{A_o}\right) \quad (5)$$

The kinetics parameters values were calculated by fitting linear plot as shown (Fig. 4 a-d). The various parameters are listed in (Table 2). As per fittings data, the R^2 value is more for PSO than PFO kinetics model for both AMX and AZI antibiotics, confining the chemisorption degradation of both antibiotics.

3.9. Photocatalytic degradation of malachite green (MG) and methyl Orange (MO) by TZG- NCs

The photocatalytic degradation of MO and MG dyes were examined at λ_{max} 463 and 617 nm respectively (Fig. 5 a-b), which were decreased with reaction time. The % degradation efficiency with time are presented in (Fig. 5 c-e). It was analyzed that the MO dye was degraded up to 48 % and 50.06 % in 200 min, while MG was degraded 98 % during adsorption and remaining upto 98.84 % and 99.99 % in 11 min with TZ and TZG-NCs respectively during light exposure. The faster adsorption and degradation of MG dye is due to its cationic nature which adsorb due to electrostatic interactions, while MO dye is an anionic dye and consist electrostatic repulsion with TZ and TZG-NCs and obtained less adsorption [65]. In general, "More the adsorption leads the more photocatalytic activity".

The kinetic parameters for both the PFO and PSO models were determined by linear plotting, as illustrated in Fig. 6 (a-d). The corresponding parameter values are summarized in Table 1. Based on the data, the PFO model shows higher R^2 values compared to the PSO model for the degradation of MO and MG dyes on TZG-NCs, indicating a better fit with the PFO model.

3.10. Antibacterial activity

To investigate the health and environmental effects of the materials, antibacterial activity towards both Gram (+ve) and Gram (−ve) bacteria using a disc diffusion method, and the results are presented in (Fig. 7 a-f).

The TZG-NCs showed excellent antimicrobial activity towards *S. aureus*, *Streptococcus sp.* (Gram + ve bacteria) and *E. coli, K. pneumonias, P. aeruginosa and S. typhii* (Gram –ve bacteria) shown in (Fig. 7 a-f). The inhibition zones are (20.1 ± 0.14 mm), (11.5 ± 0.35 mm), (10.3 ± 0.84 mm), (23.0 ± 0.42 mm), (20.0 ± 0.28 mm), (23.0 ± 0.42 mm), and (15.2 ± 0.21 mm) with TZG NCs for *S. aureus*, *Streptococcus sp.* and

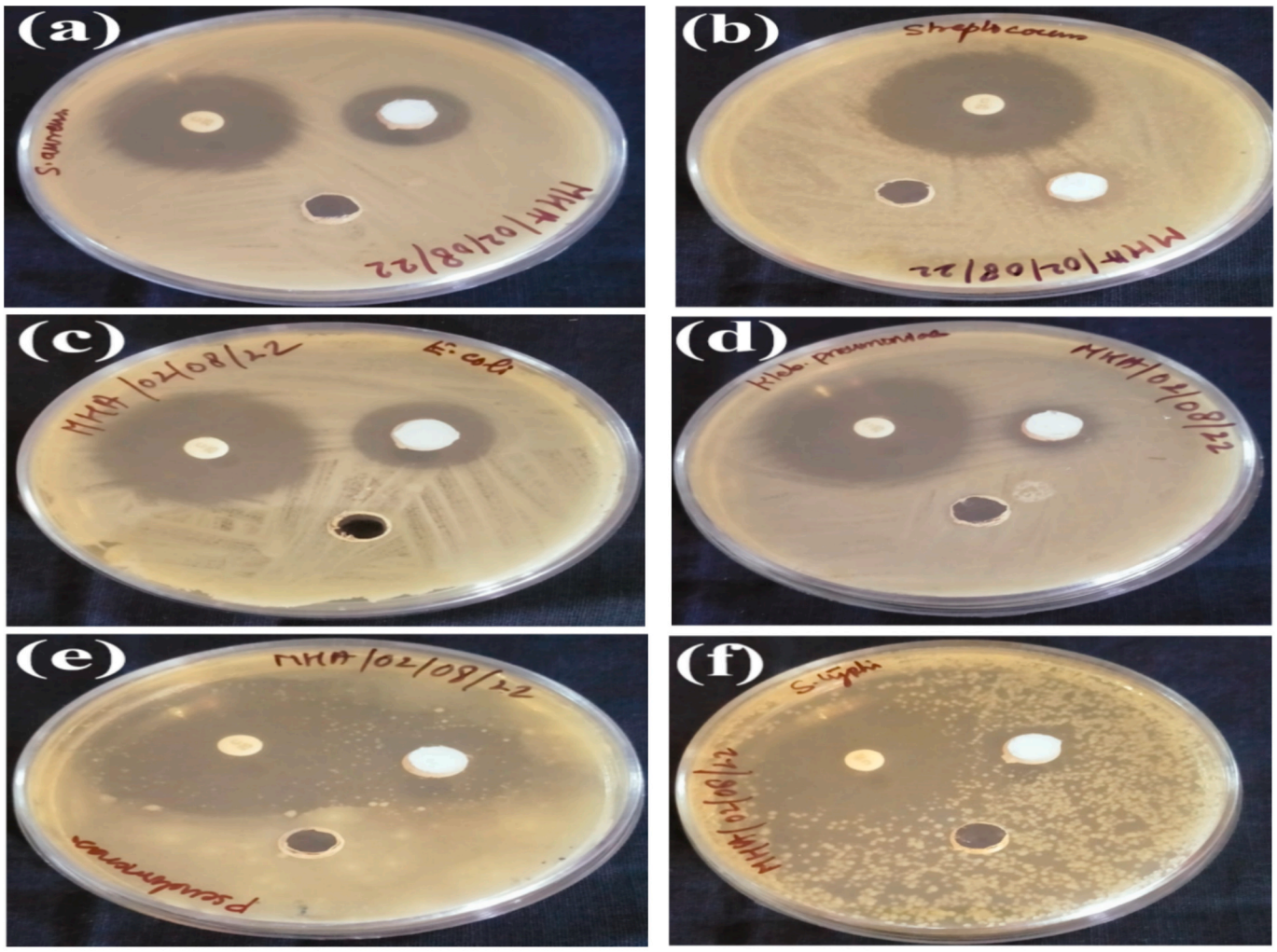

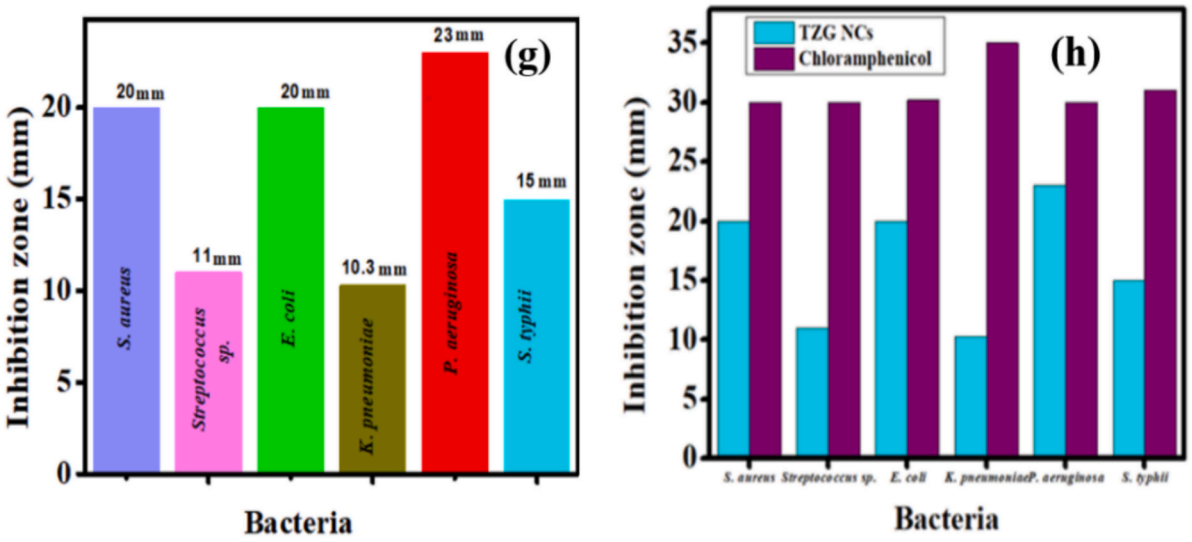

Fig. 7. Antibacterial activity of TZG-NCs against: (Gram + *ve* bacteria) a) *Staphylococcus aureus*. b) *Streptococcus sp.* (Gram – *ve* bacteria), c) *Escherichia coli.* d) *Klebsiella pneumoniae.* e) *Pseudomonas aeruginosa.* f) *Salmonella typhii.* g) Inhibition zone (mm). h) Comparison of Inhibition zone (mm) by TZG-NCs and Chloramphenicfol as control drug.

Table 3
Antibacterial performance of TZG-NCs against Gram (+ve) and Gram (−ve) bacteria.

Bacteria	Inhibition zone (mm)	
	TZG-NCs	Chloramphenicol
Staphylococcus aureus	20.1 ± 0.14	30 ± 0.28
Streptococcus sp.	11.5 ± 0.35	30.0 ± 0.0
Escherichia coli	20.0 ± 0.28	30.2 ± 0.14
Klebsiella pneumoniae	10.3 ± 0.84	35.0 ± 0.0
Pseudomonas aeruginosa	23.0 ± 0.42	30.0 ± 0.0
Solmenella typhii	15.2 ± 0.21	31.0 ± 0.0

E. coli, K. pneumoniae, P. aeruginosa and S. typhii respectively which is comparable with standard drug Chloramphenicol (Fig. 7 g-h) (Table 3). Among all tested bacteria the maximum inhibition zone was observed for *P. aeruginosa* (23.0 ± 0.42 mm) (Fig. 7 g).

3.11. Mechanism for dye degradation

As illustrated in Fig. 8, the adsorption process of MG/MO dyes, particularly MG, on the surface of TZG NCs can be explained as follows: (i) MG contains three aromatic rings and two –N—C–C—C– bonds, while GO possesses delocalized conjugated π electrons and oxygen-containing groups, facilitating π-π interactions. (ii) When dissolved in water, MG's protonated amino group interacts with the GO surface through cation-π bonding. (iii) Electrostatic attraction occurs between the positively charged MG molecules and the oxygen-containing groups in GO, TiO_2, and ZnO [66]. In general, the energy levels follow the order ZnO (CB) > TiO_2 (CB) > GO. [54]. Upon solar irradiation, TZG NCs are excited, leading to the generation of electron-hole (e^-/h^+) pairs. Electrons move from the valence band (VB) to the conduction band (CB) [67]. Specifically, electrons transfer from the CB of ZnO (−0.33 eV) to the CB of TiO_2 (−0.20 eV), and subsequently to the GO nanosheets. Simultaneously, holes (h^+) transfer from the VB of TiO_2 (+2.87 eV) to the VB of ZnO (+2.82 eV). This efficient separation of e^-/h^+ pairs reduces recombination, enhancing the photocatalytic efficiency of TZG NCs. The generated superoxide $O_2^{\cdot -}$ and hydroxyl $OH^{\cdot}$ radicals are responsible for the effective photocatalytic degradation of pollutants [68].LC-MS data and probable pathway of MG dyes is presented in Fig. 7-8S. Few major peaks are not presented in degraded dye indicated degradation of dye in presence of photocatalyst. Probable mechanism is given in eq. 6–12.

$$TZG + h\nu \rightarrow h^+ + e^- \quad (6)$$

$$h^+ + H_2O \rightarrow OH^{\cdot} + H^{+}h^+ + H_2O \rightarrow OH^{\cdot} + H^+ \quad (7)$$

$$O_2^{\cdot -} + 2\dot{H} \rightarrow H_2O_2 + O_2 \quad (8)$$

$$H_2O_2 + h\nu \rightarrow 2OH \quad (9)$$

$$OH^{\cdot} + MO/MG\ Dye \rightarrow Degraded\ Products \quad (10)$$

$$e^- + O_2 \rightarrow O_2^{\cdot -} \quad (11)$$

$$O_2^{\cdot -} + MO/MG\ Dye \rightarrow Degraded\ Products \quad (12)$$

3.12. Effect of scavengers and recyclability

The mechanism is studied by using scavengers for MO and MG dyes. In this degradation process, the dye solution (1×10^{-5} M) was with the TZG-NCs (0.1 g/100 mL of reaction solution). The selected scavengers (10^{-3} mol/L) were *i*-propyl alcohol, $AgNO_3$, and EDTA for $OH^{\cdot}$, $O_2^{\cdot -}$, h^+, respectively. The percentage removal for MO dye was found 50.06 % for TZG-NCs when no scavengers were added. It was observed that degradation was declined from 50 % to 12 %, 13 % and 19.6 % with the addition of i-propyl alcohol, $AgNO_3$ and EDTA scavengers respectively (Fig. 6S a). But in the case of MG dye (1×10^{-5} M) degradation was 99.99 % which falls to 44.5 %, 34 % and 66 % on using scavengers *i*-propyl alcohol, $AgNO_3$ and EDTA, respectively (Fig. 6S b). In all the cases, the degradation was declined when the scavengers were added which confirms that all the intermediates like $OH^{\cdot}$, $O_2^{\cdot -}$ and h^+ plays an important role during the photocatalytic process. On the basis of all observations, photocatalytic degradation is controlled by both charge carriers and radicals.

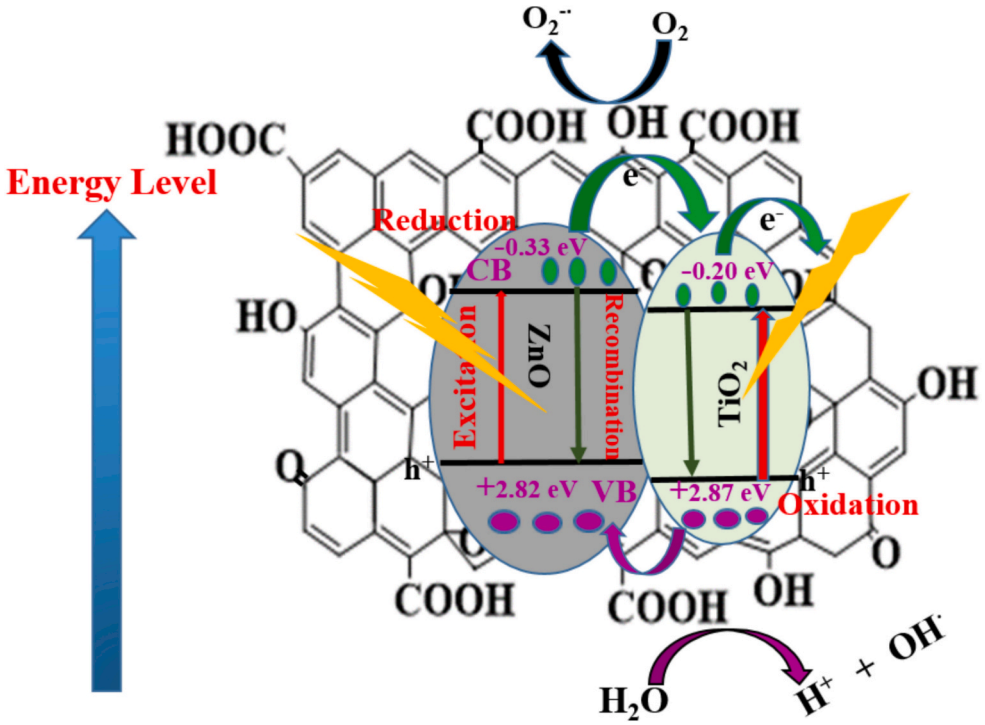

Fig. 8. Mechanism of Photocatalytic degradation of MO/MG dyes with TZG-NCs.

Recyclability tests were done in 5 cycles of MO and MG dyes solution with TZG-NCs. After every cycle, C_2H_5OH and DI water were used for washing the photocatalyst then dry in oven and used it again for next cycle. The regeneration efficiencies of photocatalyst for the five continuous cycles for MO and MG dye degradation is shown in (Fig. 6S c-d). There were almost 20 % drop in the MO dye efficiency while 2–3 % loss was observed which concluded that TZG-NCs photocatalyst can be reused multiple times without any significant lose in efficiency.

4. Conclusions

In summary, TZG NCs were synthesized *via* a simple and efficient route for the effective degradation of antibiotics and dyes. The photocatalytic degradation efficiencies of TZG-NCs for AMX and AZI antibiotics, and MO and MG dyes were 88 %, 50 % and 50.06 %, and 99.99 %, respectively, with MG dye degrading the fastest (99.99 %). The antimicrobial activity of TZG NCs was evaluated, showing excellent results against Gram-positive and Gram-negative bacteria, with the highest inhibition zone (23 ± 0.42 mm) observed for *P. aeruginosa*. The photocatalytic degradation followed PSO kinetics for antibiotics (AMX and AZI) and PFO kinetics for dyes (MO and MG). The degradation mechanism confirmed the involvement of $\dot{OH}$, $O_2^{\cdot -}$, h^+ scavengers. The excellent reusability of TZG NCs highlights its potential as an efficient photocatalyst for antibiotics and dye degradation.

CRediT authorship contribution statement

Nidhi Verma: Writing – original draft, Formal analysis, Data curation. **Tejpal Singh Chundawat:** Supervision. **Harish Chandra:** Investigation, Formal analysis. **Monu Verma:** Validation, Investigation. **Hyunook Kim:** Writing – review & editing. **Dipti Vaya:** Writing – review & editing, Supervision, Conceptualization.

Declaration of competing interest

The authors declare that they have no known competing financial interests or personal relationships that could have appeared to influence the work reported in this paper.

Acknowledgements

Authors are thankful to Manipal University, Jaipur, STIC Kerala, The Northcap University, Amity University Haryana for providing research facility. DV would like to acknowledge the favour provided under the DST-FIST Grant No.SR/FST/PS-I/2018/48 and SR/FST/CS-I/2022/263 Govt. of India. H. Kim is supported by the Korea Environment Industry & Technology Institute (KEITI) through the Development of Demonstration Technology for Converting Unconventional Waste Biomass to Energy, funded by the Korea Ministry of Environment (MOE) (2022003480001). M. Verma would like to thanks to National Research Foundation of Korea (NRF) for providing funding under Brain Pool (BP) Program (RS-2024-00406513).

Appendix A. Supplementary data

Supplementary data to this article can be found online at https://doi.org/10.1016/j.jwpe.2025.107647.

Data availability

No data was used for the research described in the article.

References

[1] C.B. Ong, L.Y. Ng, A.W. Mohammad, A review of ZnO nanoparticles as solar photocatalysts: synthesis, mechanisms and applications, Renew. Sust. Energ. Rev. 81 (2018) 536–551, https://doi.org/10.1016/j.rser.2017.08.020.
[2] M.A. Shannon, P.W. Bohn, M. Elimelech, J.G. Georgiadis, B.J. Marĩas, A.M. Mayes, Science and technology for water purification in the coming decades, Nature 452 (2008) 301–310, https://doi.org/10.1038/nature06599.
[3] G.K. Ramesha, A. Vijaya Kumara, H.B. Muralidhara, S. Sampath, Graphene and graphene oxide as effective adsorbents toward anionic and cationic dyes, J. Colloid Interface Sci. 361 (2011) 270–277, https://doi.org/10.1016/j.jcis.2011.05.050.
[4] R. Yuan, Y. Zhu, B. Zhou, J. Hu, Photocatalytic oxidation of sulfamethoxazole in the presence of TiO2: effect of matrix in aqueous solution on decomposition mechanisms, Chem. Eng. J. 359 (2019) 1527–1536, https://doi.org/10.1016/j.cej.2018.11.019.
[5] S. Ma, S. Zhan, Y. Jia, Q. Shi, Q. Zhou, Enhanced disinfection application of ag-modified g-C3N4 composite under visible light, Appl. Catal. B Environ. 186 (2016) 77–87, https://doi.org/10.1016/j.apcatb.2015.12.051.
[6] D. Huang, C. Hu, G. Zeng, M. Cheng, P. Xu, X. Gong, R. Wang, W. Xue, Combination of Fenton processes and biotreatment for wastewater treatment and soil remediation, Sci. Total Environ. 574 (2017) 1599–1610, https://doi.org/10.1016/j.scitotenv.2016.08.199.
[7] F. Mostafa, Al-Hakkani, HPLC analytical method validation for determination of cefotaxime in the bulk and finished pharmaceutical dosage form, Sustainable Chemical Engineering (2020) 33–42, https://doi.org/10.37256/sce.112020199.33-42.
[8] M.H. Abdurahman, A.Z. Abdullah, N.F. Shoparwe, A comprehensive review on sonocatalytic, photocatalytic, and sonophotocatalytic processes for the degradation of antibiotics in water: synergistic mechanism and degradation pathway, Chem. Eng. J. 413 (2021) 127412, https://doi.org/10.1016/j.cej.2020.127412.
[9] M. Čizmić, D. Ljubas, M. Rožman, D. Ašperger, L. Ćurković, S. Babíc, Photocatalytic degradation of azithromycin by nanostructured TiO 2 film: kinetics, degradation products, and toxicity, Materials 16 (2019), https://doi.org/10.3390/ma12060873.
[10] M. Usman, M. Farooq, K. Hanna, Environmental side effects of the injudicious use of antimicrobials in the era of COVID-19, Sci. Total Environ. 745 (2020) 141053, https://doi.org/10.1016/j.scitotenv.2020.141053.
[11] M.A.B. Lucien, M.F. Canarie, P.E. Kilgore, G. Jean-Denis, N. Fénélon, M. Pierre, M. Cerpa, G.A. Joseph, G. Maki, M.J. Zervos, P. Dely, J. Boncy, H. Sati, A. del Rio, P. Ramon-Pardo, Antibiotics and antimicrobial resistance in the COVID-19 era: perspective from resource-limited settings, Int. J. Infect. Dis. 104 (2021) 250–254, https://doi.org/10.1016/j.ijid.2020.12.087.
[12] S. Chandra, P. Jagdale, I. Medha, A.K. Tiwari, M. Bartoli, A. De Nino, Olivitoetal Biochar-Supported TiO2-Based Nanocomposites for the Photocatalytic degradation of sulfamethoxazole in water —, A Review 9 (11) (2021) 313, https://doi.org/10.3390/toxics9110313.
[13] P. de Abreu, E.L. Pereira, C.M.M. Campos, F.L. Naves, Photocatalytic oxidation process (UV/H2O2/ZnO) in the treatment and sterilization of dairy wastewater, Acta Scientiarum - Technology 35 (2013) 75–81, https://doi.org/10.4025/actascitechnol.v35i1.11132.
[14] J.J. Murcia, M. Hernández-Laverde, H. Rojas, E. Muñoz, J.A. Navío, M.C. Hidalgo, Study of the effectiveness of the flocculation-photocatalysis in the treatment of wastewater coming from dairy industries, J. Photochem. Photobiol. A Chem. 358 (2018) 256–264, https://doi.org/10.1016/j.jphotochem.2018.03.034.
[15] A. Jain, D. Vaya, Photocatalytic activity of TiO2 Nanaomaterial, J. Chil. Chem. Soc. 4 (2017) 3683–3690.
[16] R. Yadav, T.S. Chundawat, P.K. Surolia, D. Vaya, Photocatalytic degradation of Ortho-Nitrophenol using ZnO-β-CD nanocomposite, ChemistrySelect 7 (2022), https://doi.org/10.1002/slct.202200394.
[17] A. Sharma, B.K. Lee, Integrated ternary nanocomposite of TiO2/NiO/reduced graphene oxide as a visible light photocatalyst for efficient degradation of o-chlorophenol, J. Environ. Manag. 181 (2016) 563–573, https://doi.org/10.1016/j.jenvman.2016.07.016.
[18] V.D. Potle, S.R. Shirsath, B.A. Bhanvase, V.K. Saharan, Sonochemical preparation of ternary rGO-ZnO-TiO2 nanocomposite photocatalyst for efficient degradation of crystal violet dye, Optik 208 (2020), https://doi.org/10.1016/j.ijleo.2020.164555.
[19] Z. Li, M. Qi, C. Tu, W. Wang, J. Chen, A.J. Wang, Highly efficient removal of chlorotetracycline from aqueous solution using graphene oxide/TiO 2 composite: properties and mechanism, Appl. Surf. Sci. 425 (2017) 765–775, https://doi.org/10.1016/j.apsusc.2017.07.027.
[20] P. Tabrizian, W. Ma, A. Bakr, M.S. Rahaman, pH-sensitive and magnetically separable Fe/cu bimetallic nanoparticles supported by graphene oxide (GO) for high-efficiency removal of tetracyclines, J. Colloid Interface Sci. 534 (2019) 549–562, https://doi.org/10.1016/j.jcis.2018.09.034.
[21] N.P. Rajkumari, A. Rouf, P. Dutta, P. Goswami, Synchronizing charge-carrier capacity and interfacial morphology of green rGO modified ZnO and TiO2 heterojunctions and study of their photocatalytic behaviour towards UV and visible light active drug and dye, Materials Science and Engineering B: Solid-State Materials for Advanced Technology 287 (2023), https://doi.org/10.1016/j.mseb.2022.116094.
[22] A.A. Manda, S.A. Haladu, K.A. Elsayed, U. Ibrahim Gaya, M. Alheshibri, A. Al Baroot, E. Çevik, İ. Ercan, F. Ercan, T.S. Kayed, S. Musa Magami, N.A. Altamimi, Fast one-pot laser-based fabrication of ZnO/TiO2-reduced graphene oxide nanocomposite for photocatalytic applications, Opt. Laser Technol. 160 (2023), https://doi.org/10.1016/j.optlastec.2022.109105.

[23] P.N. Rudd, S.J. Tereniak, R. Lopez, Characterizing density and SpatialDistribution of trap states in Ta_3N_5 thin films for rational defect passivation, Appl. Mater. Interfaces 15 (2023) 7969–7977, https://doi.org/10.1021/acsami.2c19275.

[24] R. Liu, H. Ye, X. Xiong, H. Liu, Fabrication of TiO2/ZnO composite nanofibers by electrospinning and their photocatalytic property, Mater. Chem. Phys. 121 (2010) 432–439, https://doi.org/10.1016/j.matchemphys.2010.02.002.

[25] B. Bethi, S.H. Sonawane, I. Potoroko, B.A. Bhanvase, S.S. Sonawane, Novel hybrid system based on hydrodynamic cavitation for treatment of dye waste water: a first report on bench scale study, journal of environmental, Chem. Eng. 5 (2017) 1874–1884, https://doi.org/10.1016/j.jece.2017.03.026.

[26] T.P. Shende, B.A. Bhanvase, A.P. Rathod, D.V. Pinjari, S.H. Sonawane, Sonochemical synthesis of graphene-Ce-TiO2 and graphene-Fe-TiO2 ternary hybrid photocatalyst nanocomposite and its application in degradation of crystal violet dye, Ultrason. Sonochem. 41 (2018) 582–589, https://doi.org/10.1016/j.ultsonch.2017.10.024.

[27] R. Yan, X. Son, X. Wang, Q. Peng, Y. Li, Crystal structures, anisotropic growth, and optical properties: controlled synthesis of lanthanide orthophosphate one-dimensional nanomaterials, Chem. Eur. J. 11 (2005) 2183–2195, https://doi.org/10.1002/chem.200400649.

[28] D.L. Liao, C.A. Badour, B.Q. Liao, Preparation of nanosized TiO2/ZnO composite catalyst and its photocatalytic activity for degradation of methyl orange, J. Photochem. Photobiol. A Chem. 194 (2008) 11–19, https://doi.org/10.1016/j.jphotochem.2007.07.008.

[29] S.H. Hwang, J. Song, Y. Jung, O.Y. Kweon, H. Song, J. Jang, Electrospun ZnO/TiO2 composite nanofibers as a bactericidal agent, Chem. Commun. 47 (2011) 9164–9166, https://doi.org/10.1039/c1cc12872h.

[30] M.F. Abdel Messih, M.A. Ahmed, A. Soltan, S.S. Anis, Facile approach for homogeneous dispersion of metallic silver nanoparticles on the surface of mesoporous titania for photocatalytic degradation of methylene blue and indigo carmine dyes, J. Photochem. Photobiol. A Chem. 335 (2017) 40–51, https://doi.org/10.1016/j.jphotochem.2016.11.001.

[31] M.K. Kavitha, P. Gopinath, H. John, Reduced graphene oxide-ZnO self-assembled films: tailoring the visible light photoconductivity by the intrinsic defect states in ZnO, Phys. Chem. Chem. Phys. 17 (2015) 14647–14655, https://doi.org/10.1039/c5cp01318f.

[32] S. Banerjee, S.C. Pillai, P. Falaras, K.E. O'shea, J.A. Byrne, D.D. Dionysiou, New insights into the mechanism of visible light photocatalysis, J. Phys. Chem. Lett. 5 (2014) 2543–2554, https://doi.org/10.1021/jz501030x.

[33] Z. Liu, X. Zhang, B. Wang, M. Xia, S. Gao, X. Liu, A. Zavabeti, J.Z. Ou, K. Kalantar-Zadeh, Y. Wang, Amorphous MoSx-coated TiO2 nanotube arrays for enhanced Electrocatalytic hydrogen evolution reaction, J. Phys. Chem. C 122 (2018) 12589–12597, https://doi.org/10.1021/acs.jpcc.8b01678.

[34] X. Chen, L. Liu, P.Y. Yu, S.S. Mao, Increasing solar absorption for photocatalysis with black hydrogenated titanium dioxide nanocrystals, Science 331 (2011) 746–750, https://doi.org/10.1126/science.1200448.

[35] Y. Chen, S. Tan, F. Yang, Z. Chen, Z. Wu, J. Huang, Soluble expression and purification of a functional harpin protein in Escherichia coli, Process Biochem. 57 (2017) 200–206, https://doi.org/10.1016/j.procbio.2017.03.010.

[36] Z. Jie, L. Yang, T. Huiyuan, X. Mengyan, D. Xiuhong, W. Zehua, L. Chunguang, D. Xianying, C. Jiehu, Layered by layered construction of three novel ZnCo-LDHs/g-C3N4 for the removal of sunset yellow by adsorption-photocatalytic process, Environ. Sci. Pollut. Res. 30 (2023) 100450–100465, https://doi.org/10.1007/s11356-023-29347-2.

[37] Y. Gong, X. Ma, R. Dang, J. Liu, J. Cao, Synthesis of highly dispersed and versatile anatase TiO2 nanocrystals on graphene sheets with enhanced photocatalytic performance for dye degradation, J. Mater. Sci. Mater. Electron. 28 (2017) 18883–18890, https://doi.org/10.1007/s10854-017-7841-2.

[38] S. Lv, J. Wan, Y. Shen, Z. Hu, Preparation of superlong TiO2 nanotubes and reduced graphene oxide composite photocatalysts with enhanced photocatalytic performance under visible light irradiation, J. Mater. Sci. Mater. Electron. 28 (2017) 14769–14776, https://doi.org/10.1007/s10854-017-7346-z.

[39] R.K. Upadhyay, N. Soin, S.S. Roy, Role of graphene/metal oxide composites as photocatalysts, adsorbents and disinfectants in water treatment: a review, RSC Adv. 4 (2014) 3823–3851, https://doi.org/10.1039/C3RA45013A.

[40] R. Mohammadi, B. Massoumi, M. Rabani, Photocatalytic decomposition of amoxicillin trihydrate antibiotic in aqueous solutions under UV irradiation using Sn/TiO 2 nanoparticles, International Journal of Photoenergy 2012 (2012), https://doi.org/10.1155/2012/514856.

[41] M. Verma, A.K. Haritash, Photocatalytic degradation of amoxicillin in pharmaceutical wastewater: a potential tool to manage residual antibiotics, Environ. Technol. Innov. 20 (2020) 101072, https://doi.org/10.1016/j.eti.2020.101072.

[42] L. Bergamonti, C. Bergonzi, C. Graiff, P.P. Lottici, R. Bettini, L. Elviri, 3D printed chitosan scaffolds: a new TiO2 support for the photocatalytic degradation of amoxicillin in water, Water Res. 163 (2019) 114841, https://doi.org/10.1016/j.watres.2019.07.008.

[43] A.S. Sartape, A.M. Mandhare, V.V. Jadhav, P.D. Raut, M.A. Anuse, S.S. Kolekar, Removal of malachite green dye from aqueous solution with adsorption technique using Limonia acidissima (wood apple) shell as low cost adsorbent, Arab. J. Chem. 10 (2017) S3229–S3238, https://doi.org/10.1016/j.arabjc.2013.12.019.

[44] Z.Y. Zhang, G.D. Zhang, X.X. Sheng, Q.W. Ding, Y.Z. Bai, Y. Su, H.K. Liu, Z. Su, Efficient MO dye degradation catalyst of cu(I)-based coordination complex from dissolution-recrystallization structural transformation, Crystal Growth and Design 21 (2021) 333–343, https://doi.org/10.1021/acs.cgd.0c01216.

[45] S. Li, K. Dong, M. Cai, X. Li, X. Chen, A plasmonic S-scheme au/MIL-101(Fe)/BiOBr photocatalyst for efficient synchronous decontamination of Cr(VI) and norfloxacin antibiotic, EScience 4 (2024) 100208, https://doi.org/10.1016/j.esci.2023.100208.

[46] S. Li, C. Wang, K. Dong, P. Zhang, X. Chen, X. Li, MIL-101(Fe)/BiOBr S-scheme photocatalyst for promoting photocatalytic abatement of Cr(VI) and enrofloxacin antibiotic: performance and mechanism, Chin. J. Catal. 51 (2023) 101–112, https://doi.org/10.1016/S1872-2067(23)64479-1.

[47] C. Shen, X. Li, B. Xue, D. Feng, Y. Liu, F. Yang, M. Zhang, S. Li, Surface plasmon effect combined with S-scheme charge migration in flower-like ag/Ag6Si2O7/Bi12O17Cl2 enables efficient photocatalytic antibiotic degradation, Appl. Surf. Sci. 679 (2025) 161303, https://doi.org/10.1016/j.apsusc.2024.161303.

[48] M. Cai, Y. Liu, K. Dong, X. Chen, S. Li, Floatable S-scheme Bi2WO6/C3N4/carbon fiber cloth composite photocatalyst for efficient water decontamination, Chin. J. Catal. 52 (2023) 239–251, https://doi.org/10.1016/S1872-2067(23)64496-1.

[49] S. Li, C. You, Q. Xue, Y. Zhao, F. Yang, Y. Liu, L. Bai, M. Zhang, C. Zhuang, Carbon quantum dots and interfacial chemical bond synergistically modulated S-scheme Mn0.5Cd0.5S/BiOBr photocatalyst for efficient water purification, J. Mater. Sci. Technol. 214 (2025) 255–265, https://doi.org/10.1016/j.jmst.2024.07.015.

[50] S. Li, R. Yan, M. Cai, W. Jiang, M. Zhang, X. Li, Enhanced antibiotic degradation performance of Cd0.5Zn0.5S/Bi2MoO6 S-scheme photocatalyst by carbon dot modification, J. Mater. Sci. Technol. 164 (2023) 59–67, https://doi.org/10.1016/j.jmst.2023.05.009.

[51] K. Dong, C. Shen, R. Yan, Y. Liu, C. Zhuang, S. Li, Integration of Plasmonic effect and S-scheme heterojunction into ag/Ag3PO4/C3N5 Photocatalyst for boosted photocatalytic levofloxacin degradation, Acta Phys. -Chim. Sin. 40 (2024) 2310013, https://doi.org/10.3866/PKU.WHXB202310013.

[52] D. Naghipour, K. Taghavi, J. Jaafari, I. Kabdaşlı, M. Makkiabadi, M. Javan Mahjoub Doust, F. Javan Mahjoub Doust, Scallop shell coated Fe 2 O 3 nanocomposite as an eco-friendly adsorbent for tetracycline removal, Environ. Technol. 44 (2023) 150–160, https://doi.org/10.1080/09593330.2021.1966105.

[53] D. Naghipour, L. Hoseinzadeh, K. Taghavi, J. Jaafari, A. Amouei, Effective removal of tetracycline from aqueous solution using biochar prepared from pine bark: isotherms, kinetics and thermodynamic analyses, Int. J. Environ. Anal. Chem. 103 (2023) 5706–5719, https://doi.org/10.1080/03067319.2021.1942462.

[54] S. Li, C. You, F. Yang, G. Liang, C. Zhuang, X. Li, Interfacial Mo–S bond modulated S-scheme Mn0.5Cd0.5S/Bi2MoO6 heterojunction for boosted photocatalytic removal of emerging organic contaminants, Chin. J. Catal. 68 (2025) 259–271, https://doi.org/10.1016/S1872-2067(24)60181-6.

[55] C. You, C. Wang, M. Cai, Y. Liu, B. Zhu, S. Li, Improved photo-carrier transfer by an internal electric field in BiOBr/N rich C3N5 3D/2D S-scheme heterojunction for efficiently photocatalytic micropollutant removal, Acta Phys. Sin. 40 (2024) 2407014–2407125, https://doi.org/10.3866/PKU.WHXB202407014.

[56] N. Verma, T.S. Chundawat, H. Chandra, D. Vaya, An efficient time reductive photocatalytic degradation of carcinogenic dyes by TiO2-GO nanocomposite, Mater. Res. Bull. (2022) 112043, https://doi.org/10.1016/J.MATERRESBULL.2022.112043.

[57] G.K. Upadhyay, J.K. Rajput, T.K. Pathak, V. Kumar, L.P. Purohit, Synthesis of ZnO: TiO2 nanocomposites for photocatalyst application in visible light, Vaccum 160 (2019) 154–163, https://doi.org/10.1016/j.vacuum.2018.11.026.

[58] U. Holzwarth, N. Gibson, The Scherrer equation versus the "Debye-Scherrer equation," Nat. Nanotechnol. 6 (2011) 534. doi:https://doi.org/10.1038/nnano.2011.145.

[59] M.G. Maya, S.C. George, T. Jose, L. Kailas, S. Thomas, Development of a flexible and conductive elastomeric composite based on chloroprene rubber, Polym. Test. 65 (2018) 256–263, https://doi.org/10.1016/j.polymertesting.2017.12.006.

[60] K. Zhou, Y. Zhu, X. Yang, X. Jiang, C. Li, Preparation of graphene-TiO2 composites with enhanced photocatalytic activity, New J. Chem. 35 (2011) 353–359.

[61] [59] S. Pu, R. Zhu, H. Ma, D. Deng, X. Pei, F. Qi, W. Chu, Facile in-situ design strategy to disperse TiO2 nanoparticles on graphene for the enhanced photocatalytic degradation of rhodamine 6G, Appl. Catal. B Environ. 218 (2017) 208–219. doi:https://doi.org/10.1016/j.apcatb.2017.06.039.

[62] H. Zhang, G. Chen, D.W. Bahnemann, Photoelectrocatalytic materials for environmental applications, J. Mater. Chem. 19 (2009) 5089, https://doi.org/10.1039/b821991e.

[63] H. Van Bao, N.M. Dat, N.T.H. Giang, D.B. Thinh, L.T. Tai, D.N. Trinh, N.D. Hai, N. A.D. Khoa, L.M. Huong, H.M. Nam, M.T. Phong, N.H. Hieu, Behavior of ZnO-doped TiO2/rGO nanocomposite for water treatment enhancement, Surfaces and Interfaces 23 (2021) 100950, https://doi.org/10.1016/j.surfin.2021.100950.

[64] F. Hayati, A.A. Isari, M. Fattahi, B. Anvaripour, S. Jorfi, Photocatalytic decontamination of phenol and petrochemical wastewater through ZnO/TiO2 decorated on reduced graphene oxide nanocomposite: influential operating factors, mechanism, and electrical energy consumption, RSC Adv. 8 (2018) 40035–40053, https://doi.org/10.1039/c8ra07936f.

[65] S.A. Ong, L.N. Ho, Y.S. Wong, Comparison on biodegradation of anionic dye orange II and cationic dye methylene blue by immobilized microorganisms on spent granular activated carbon, Desalin. Water Treat. 54 (2015) 557–561, https://doi.org/10.1080/19443994.2014.880155.

[66] K. Chaudhary, N. Shaheen, S. Zulfiqar, M.I. Sarwar, M. Suleman, P.O. Agboola, I. Shakir, M.F. Warsi, Binary WO3-ZnO nanostructures supported rGO ternary nanocomposite for visible light driven photocatalytic degradation of methylene blue, Synth. Met. 269 (2020), https://doi.org/10.1016/j.synthmet.2020.116526.

[67] G. Zhu, L. Pan, T. Xu, Q. Zhao, Z. Sun, Cascade structure of TiO2/ZnO/CdS film for quantum dot sensitized solar cells, J. Alloys Compd. 509 (2011) 7814–7818, https://doi.org/10.1016/j.jallcom.2011.05.043.

[68] R. Yadav, T.S. Chundawat, P.K. Surolia, D. Vaya, Photocatalytic degradation of textile dyes using β-CD-CuO/ZnO nanocomposite, J. Phys. Chem. Solids 165 (2022), https://doi.org/10.1016/j.jpcs.2022.110691.